

Slope-based eccentric photorefraction: theoretical analysis of different light source configurations and effects of ocular aberrations

Austin Roorda and Melanie C. W. Campbell

School of Optometry, University of Waterloo, Waterloo, Ontario, Canada N2L 3G1 and Guelph-Waterloo Program for Graduate Work in Physics, University of Waterloo, Waterloo, Ontario N2L 3G1, Canada

William R. Bobier

School of Optometry, University of Waterloo, Waterloo, Ontario N2L 3G1, Canada

Received November 18, 1996; revised manuscript received May 13, 1997; accepted May 13, 1997

A geometrical-optical technique is used to predict the changes in the slope of the eccentric-photorefraction intensity profiles as a function of refractive state. We investigate how the intensity profiles vary with refractive state for different light source configurations and monochromatic aberrations in the eye. The best possible light source configuration extends from zero eccentricity (to increase sensitivity and reduce the dead zone) to a high eccentricity (to increase the working range). An advantage of using the extended light source is that the intensity profile of the eccentric-photorefraction reflex is more linear for extended sources than for point light sources. It is also shown that the change in slope with refractive state is dependent on pupil size. Furthermore, when asymmetric aberrations are present, the change in intensity profile slope with refractive state is dependent on the circumferential position of the light source, but this dependence can be resolved by averaging slope values obtained by using two sources placed on opposite sides of the pupil. The importance of this study to existing eccentric-photorefractor designs is discussed, and recommendations for improved eccentric photorefractors are suggested. © 1997 Optical Society of America [S0740-3232(97)03110-4]

Key words: Eccentric photorefraction, monochromatic aberrations, vision.

1. INTRODUCTION

Eccentric photorefraction is an objective technique for measuring the refractive state of the eye. It is remote and quick, making it a convenient technique for measuring refraction in children or uncooperative patients for which subjective techniques or even retinoscopy are difficult to perform. It is also inexpensive and easy to operate, making it ideal for screening large populations for significant refractive errors.¹ The eccentric-photorefraction technique is similar in principle to the Foucault knife-edge test for measuring aberrations. Photorefraction techniques base estimations of refractive state on the properties of the light distribution or reflex that appears in the pupil after a double passage of light through the eye's optical system. Early use of the technique based estimations of refractive state on the extent of the reflex or crescent that appeared in the pupil.²⁻⁶ Measurement of the crescent extent was based on the fact that the crescent extent increased with the refractive state of the eye. Another way to analyze the reflex in the pupil has been to measure the intensity profile of the light distribution across the pupil reflex. In this technique it was found that the slope of the intensity profile increased with increasing refractive error.⁷ Typical reflexes in the pupil for myopic and hyperopic refractive states are shown in Fig. 1. The method of measuring the refractive error of the eye based on the slope of intensity profiles obtained with eccentric photorefraction has gained in popularity since the development of eccentric photorefraction as a

screening instrument for measuring the refractive error of the eye. The slope-based measurement has advantages over conventional measurements of crescent extent because more information is used from the retinal reflex, and these types of measurements can be easily automated. Crescent-extent techniques tend to have a limited working range, and thresholding problems make them highly dependent on the particular camera system that is used.^{6,8} Slope-based eccentric photorefractors are being used by Schaeffel *et al.*⁹ and are incorporated in commercial instruments, specifically the Fortune Optical (Tomey ViVA) VRB-100¹⁰ and the Topcon PR-1000/PR-2000 video refractors.^{7,11} To our knowledge, there has been limited theoretical analysis of the change in slope with refractive error¹² and no analysis of the effects of light source configuration on the slope of the reflex. Users of these instruments have always had to rely on calibration obtained from empirical investigations.⁹

In this paper we investigate the effects of different light source configurations on changes in slope of the eccentric-photorefraction intensity profile. The analysis also compares the effects of zero aberrations, symmetric aberrations, and asymmetric aberrations on the measurements. Formulas for determining the crescent extent were found to be dependent on the pupil size.^{4,5} Here we simulate changing slope with refractive error with different pupil sizes to investigate whether there are similar dependencies for slope-based photorefractors. Finally, the overall results are discussed with respect to the existing

eccentric-photorefractor designs along with proposals for improved slope-based photorefractor designs.

A. Background of Slope-Based Eccentric Photorefraction

The first mention of relating the slope of the intensity profile to refractive error was made in 1991 by Uozato *et al.*, who developed the Topcon Corporation PR-1000 infrared videorefractor.⁷ This abstract stated that “the gradient of intensity distribution in the pupil area is proportional to the refractive error of the eye.” Subsequent development of the PR-2000 (Topcon Corporation) appeared to have a similar design.¹¹

Schaeffel *et al.*¹³ designed an infrared photoretinoscope in which rows of light-emitting diodes (LED’s) at varying eccentricity were run cyclically. In 1991 they presented an automated instrument that measured the crescent size at the “half-height brightness,” using a single row of light sources at 15 mm eccentricity.¹⁴ By 1993 the design had changed so that all the LED’s were run simultaneously, and the slope of the profile was measured.⁹ The calibration curves for changing slope with refractive state were shown empirically to be relatively linear over ± 5 diopters (D) of defocus. In the 1993 paper Schaeffel and coauthors stated that the use of multiple eccentricities provided a more linear slope in the intensity profiles. This was an empirical observation, but no theoretical justification was provided. A subsequent paper in 1994 showed calibration curves for four different animal species.¹⁵

The Fortune Optical (Tomey ViVA) VRB-100 videorefractor uses a single row of infrared LED’s eccentric to the aperture and bases the refractive-error estimation on the slope of the intensity profile across the pupil.¹⁰

2. GEOMETRICAL OPTICAL ANALYSIS

The optical analysis is adapted from a previous paper.¹⁶ The difference for the current analysis is that the previous analysis modeled a point light source, whereas in this paper the analysis is for a variety of light sources. The intensity profile for a single point light source is determined in a two-step process. In the first step, light is traced into the eye to project a point spread onto the retina. This retinal point spread acts as the source for the second pass. In the second step, the rays are traced from the eye back toward the eccentric photorefractor. The rays that enter the camera aperture contribute to the

intensity profile across the pupil. One of the advantages of this optical model is that all the ray tracing is done in object space. The only features of the eye that need to be known are the changes in power and aberration across the entrance pupil of the eye.⁸ An individual ray path in object space is determined by its position in the pupil and the power of the eye corresponding to this ray. The ray will cross the principal ray at a distance from the eye, k , that varies with both the paraxial refractive error and aberration of the eye (Fig. 2). In the presence of aberrations the refractive state and the far point of the eye vary as a function of ray position in the pupil.¹⁶

In this model, rays are traced in a single plane defined by three points: the center of the camera aperture, the center of the eccentric light source, and the center of the eye being measured. Intensity profiles are calculated across the pupil meridian that lies in this plane. Such an analysis does not fully model the effects of skew rays or rays from the retinal blur outside of the meridian that may contribute to the reflex. The simplified model, however, has been shown to provide reliable predictions of expected photorefraction reflexes and has led us to the assumption that most of the reflex in a single pupil meridian can be defined by ray tracing in a single plane.¹⁶ The simplified model is appropriate when the sources are colinear with the principal astigmatic meridians of the eye.

The source can be thought of as an array of point sources, each producing a unique eccentric-photorefraction intensity profile. The effect of an extended source, therefore, can be generated by adding the calculated profiles for an array of point sources, or

$$I_{\text{total}}(x) = \sum_e I_e(x), \quad (1)$$

where e is the range of eccentricities that make up the particular source, x is the position across the meridian of the pupil that has the same orientation as the line on the photorefractor joining the light source and the center of the camera aperture, I_e is the intensity profile for a single eccentricity,¹⁶ and I_{total} is the final intensity profile for the extended or multiple sources. A least-squares routine is used to determine the best-fit slope to the intensity profile for each refractive state. The quality of the fit is determined by calculating the r^2 coefficient for each of the best-fit slopes. This was done because aberrations have been

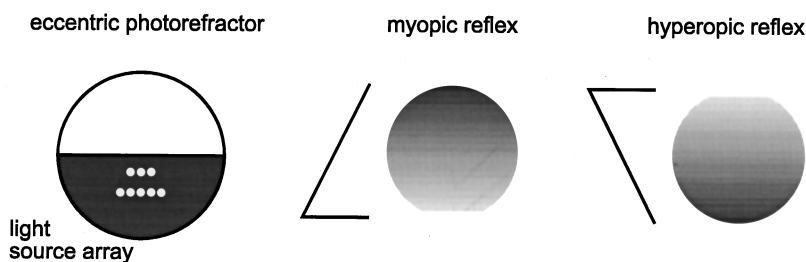


Fig. 1. Typical reflexes observed in eccentric photorefraction. The left-hand figure shows an example of a photorefractor configuration that would be used for the intensity profile measurements, based on a design by Schaeffel *et al.*¹³ The right-hand figures show the intensity distribution or reflex that appears in the pupil. The reflex fills the pupil, and the slope of the intensity profile is used to deduce the refractive state. The line to the left of each pupil shows the intensity profile across the vertical meridian of the pupil. If the eye is focused in front of the photorefractor, the reflex appears on the same side of the eye as the light source. The opposite occurs for eyes that are hyperopic with respect to the photorefractor. If the eye is focused on the photorefractor, the pupil is dim and the slope is 0.

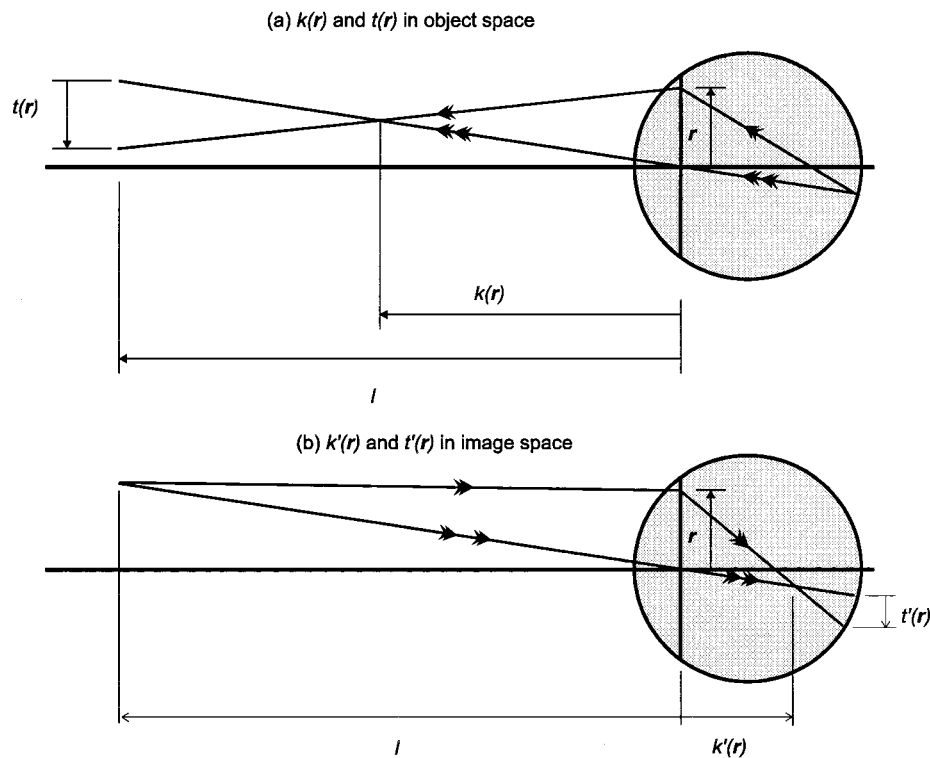


Fig. 2. (a) A ray (single arrow) emerging from a retinal point passing through the exit pupil at a radius r crosses the principal ray (double arrow) from the same retinal point at a distance $k(r)$ (the far point distance). The transverse aberration $t(r)$ is a measure of the distance from the emerging ray's intercept position to the principal ray's intercept position in a plane perpendicular to the optical axis at a specified distance l from the exit pupil. (b) The reverse situation is shown where the ray emerges from a distance l and crosses the principal ray before the retina at a distance $k'(r)$ with a transverse aberration $t'(r)$. The aberrations from object to image space are identical between conjugate planes (except for a magnification difference).²⁸ We consider only rays in a single (x) meridian.

found to cause irregular intensity profiles that are not fitted accurately with a linear function.¹⁶ The linearity of the fits is also expected to be dependent on the light source configuration. The linearity of the best-fit slope is important because a poor linear fit will be more susceptible to error caused by noise in the imaging system. All simulations were done for a pupil size of 7 mm except for the analysis of changing pupil size. All simulations were for a camera distance 1 m from the eye. Point sources were modeled at 2 mm and 8 mm eccentricity from the photorefractor. Multiple sources extended from 2 to 14 mm eccentricity and from 0 to 30 mm eccentricity. Extended sources were modeled as a line of discrete point sources at different eccentricities spanning the range of the extended source. Continuous sources were also modeled by using smaller intervals between individual point sources.

The effects of symmetric aberrations were modeled for a value of spherical aberration of 1.83 D, based on the third-order spherical aberration of the eye of one of the authors (MC)¹⁷ and deliberately chosen to be larger than the overall spherical aberration in that eye¹⁷ and larger than the spherical aberration commonly found¹⁸ in the human eye.

The effects of asymmetric aberrations were modeled by using the transverse aberration along the horizontal meridian of AR's left eye. The aberrations were measured for the eye accommodated on a 2-m target with a psycho-

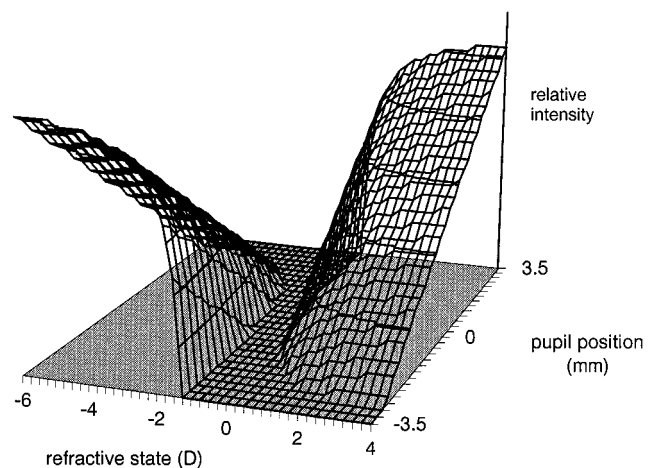


Fig. 3. Plot of eccentric-photorefractive intensity profiles as a function of refractive state. The cross sections at each refractive state of the surface plot represent the intensity across the meridian of the pupil. The intensity profiles are generated by a geometrical-optical technique.¹⁶ For myopic refractive states (negative refractive states), the intensity profiles ramp to the same side of the pupil as the eccentric light source and to the opposite side for hyperopic refractive states (positive refractive states). When the eye is focused on or near the camera (at -1 D), no intensity distribution is observed; this region is called the dead zone. This simulation is for a point light source at 2 mm eccentricity, a 1-m working distance, and a 7-mm pupil. The slopes for the intensity profiles as a function of refractive state are shown for this surface plot in Fig. 4(a).

physical technique.¹⁷ The particular aberration for AR's left eye was a combination of symmetric and asymmetric aberrations. The expression for the transverse aberration is

$$t(x) = -0.6737 - 0.1918x^3 + 0.04394x^4, \quad (2)$$

where $t(x)$ is the transverse aberration in object space (in minutes of arc) and x is the position in millimeters across the meridian of the pupil. The far point position for each ray in the pupil (Fig. 2) can be calculated from

$$k(x) = \frac{l}{\left[1 - \frac{t(x)}{x}\right]}. \quad (3)$$

From the knowledge of the position of the far point, rays can be traced to derive the intensity of the photorefractive pattern observed in the pupil.¹⁶

The calculations were iterative and were done by using a BASIC program on a 486 PC. The calculation of the profiles for a range of refractive states generally took less

than 5 min, depending on the number of rays, the size of the refractive-state increment, the size of the pupil, and the complexity of the aberration function.

3. RESULTS

Two important definitions are required at this point. The term *slope* will refer to the slope of an individual photorefractive intensity profile across the pupil. The change in the slope of the intensity profile as function of refractive state also has a slope, but this will be referred to as the *gain* so that they can be distinguished throughout the results and the discussion.

The results of the simulations are shown on Figs. 3–8. The output of the program is a series of intensity profiles across the pupil as a function of refractive state. Each intensity profile can be plotted in succession to form a surface plot showing the changing profile shape with refractive state. A typical plot is shown in Fig. 3. The slope of the profile for each refractive state is determined by doing a least-squares best-fit line to each predicted

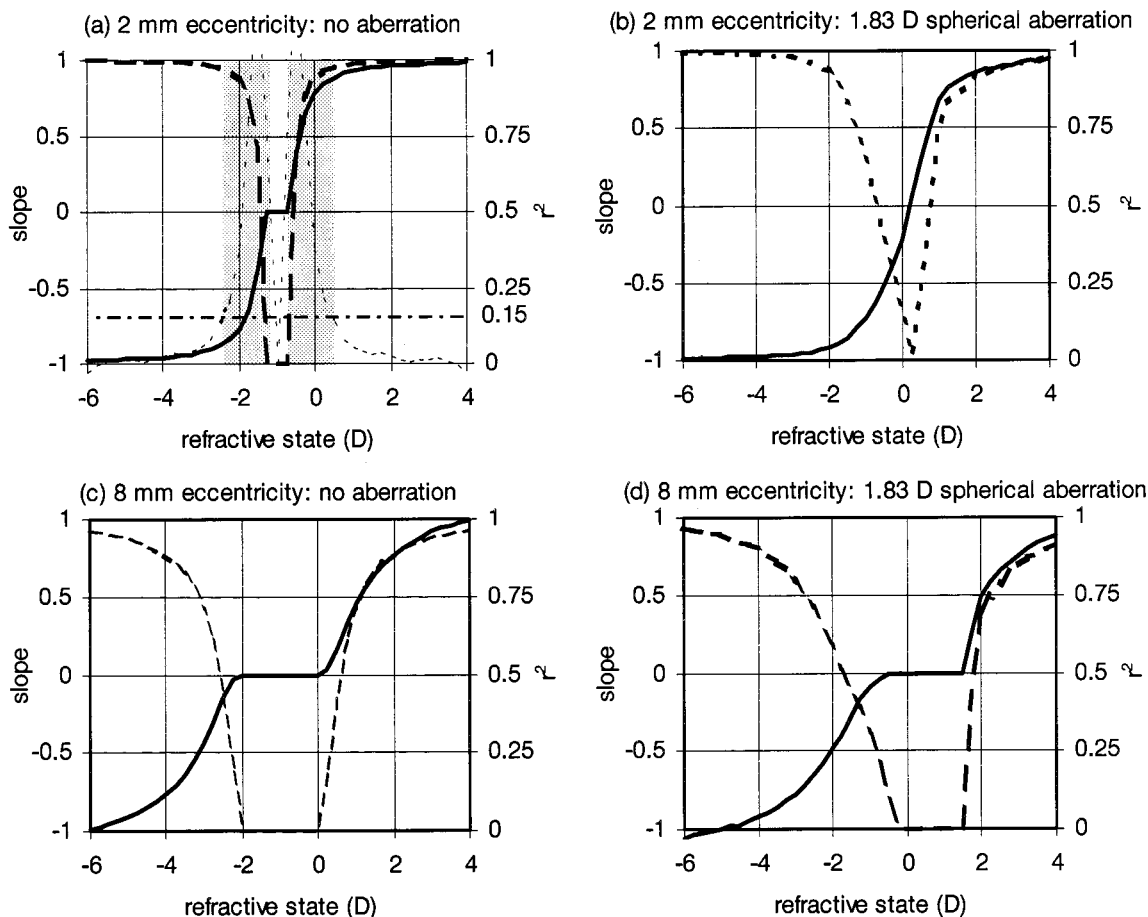


Fig. 4. Plots of eccentric-photorefractive intensity profile slopes as a function of refractive state. The solid curves represent the slope of the intensity profile as a function of refractive state (see Fig. 3). The heavy dashed curves represent the r^2 value for the best-fit line to the calculated intensity profile. (a) and (b), point light source at 2 mm eccentricity; (c) and (d), point light source at 8 mm eccentricity. In (a), the light dashed curve represents the gain (the derivative of slope with respect to refractive state). The gain versus the refractive-state curve is used to define the limits of the working range (shaded area; see Section 3). Plots (a), (c), and (d) have a region near the camera position (-1 D) for which no changes in slope with refractive state are observed. This dead zone is four times larger for the 8-mm-eccentric source than for the 2-mm-eccentric source. At the limits of the working range, the gain decreases and the slope changes very slowly with refractive state. This quick reduction in gain is referred to as saturation. In general, the fits are least linear for refractive states near the camera position.

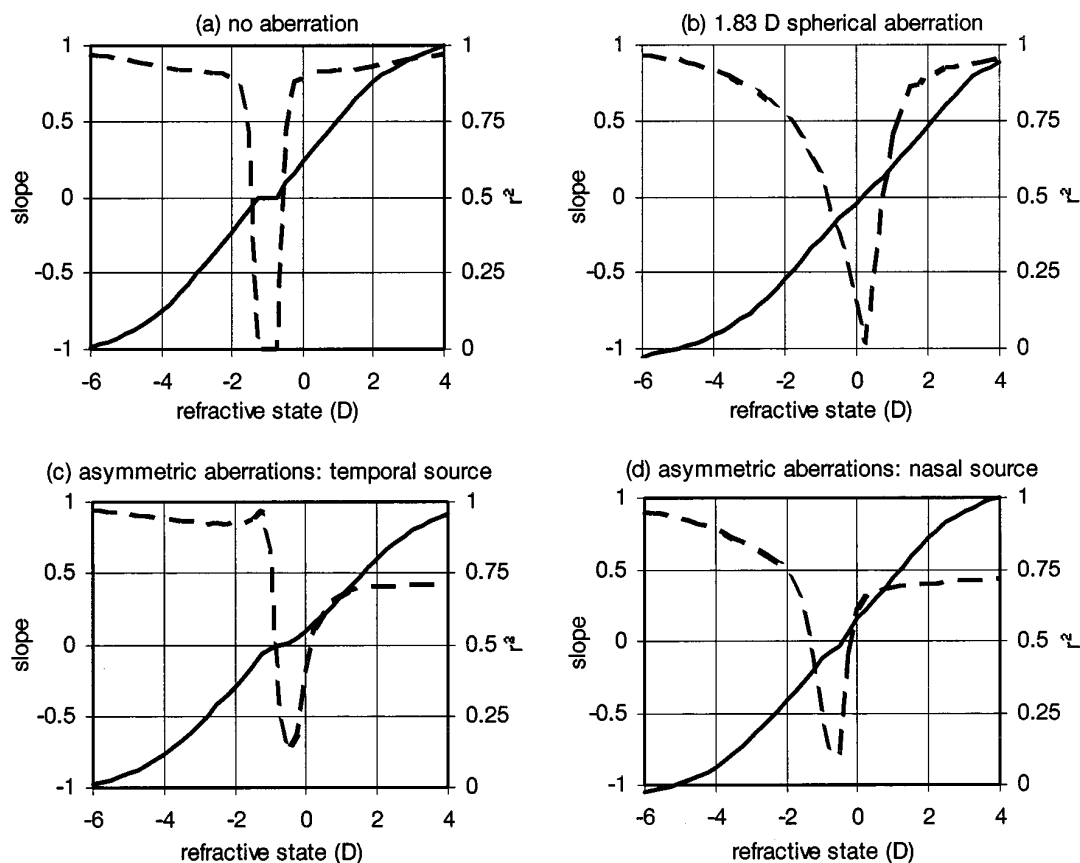


Fig. 5. Plots of slope versus refractive state for an eccentric photorefractor with an extended source made up of point sources at 2, 5, 8, 11, and 14 mm. The solid curves represent the slope of the intensity profile. The dashed curves represent the r^2 value for the slopes best fitted to the calculated intensity profile. With the extended source, the working range is increased over the point light source simulations of Fig. 4. The slopes for each of the plots have been normalized by the same value. The quality of the fits of the best-fit line to the intensity profiles are best for the no-aberration case.

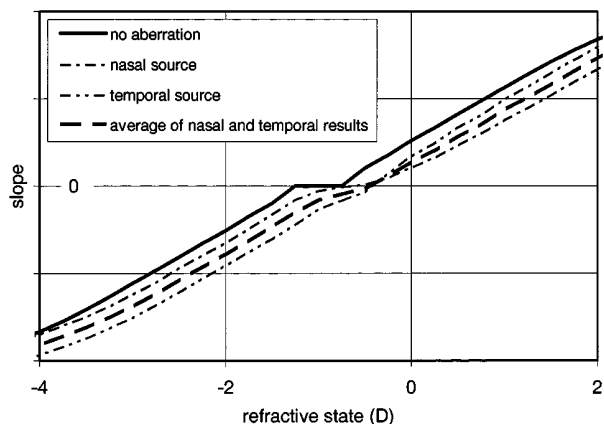


Fig. 6. Effects of asymmetric aberrations can be canceled by averaging the slope for diametrically opposite sources. The curves of slope versus refractive state from Figs. 5(c) and 5(d) are plotted and averaged. The curve for the temporal source is 11% flatter and for the nasal source is 11% steeper than in the no-aberration case. If the two are averaged, the gain is less than 1% different from the no-aberration case. In this example the curves for the combination of symmetric and asymmetric aberration are shifted toward the best focal plane for the aberrated eye.

profile. Changes in slope with refractive state are shown on the plots on Figs. 4–8. The figures are ordered so that there are point light source models first (Fig. 4), followed

by results from extended light sources (Figs. 5–7). The differences in the results between discrete point sources and continuous sources were very small, so only the simulations with the multiple point sources are presented here.¹⁹ The main difference that we observed between continuous and multiple point sources was that the continuous sources produced slightly smoother intensity profiles. This difference is not important since, in practice, the profiles tend to be smoother already as a result of intraocular scattering,²⁰ retinal spreading,²¹ multiple surfaces of reflection on the retina,²² and chromatic aberration.²³

In Figs. 4–8 the slope of the solid line represents the gain, or the change in slope of the photorefractive profile as a function of refractive state. The slope change with refractive state for all the plots was normalized by equating the maximum slope of the no-aberration condition for each configuration to 1. The slopes in all the subsequent plots with the same light source configuration were scaled by the same value. The absolute magnitude of the slope was not of interest, as that could be varied with radiant power of the light source or camera sensitivity. The long-dashed curves in Figs. 4, 6, and 8 represent the corresponding r^2 value for the best-fit slopes to each of the photorefractive profiles. The magnitude of the correlation coefficient indicates the linearity of the gradient of the in-

tensity profile across the pupil for each refractive state. Since all simulations were for a camera distance of 1 m, a myopic refractive state of -1 D indicates that the eye is focused in the camera plane. At this refractive state the photorefractor slope for the aberration-free eye would be zero (see Fig. 4).

A means of correcting for the errors caused by asymmetric aberrations is to average the slope of the intensity profile obtained with the eccentric light on either side of the limiting aperture. This is shown on Fig. 6.

The important feature of the plots is the changing gain as a function of refractive state. The working range for each photorefractor configuration was defined as the region within which there is a significant amount of gain. A quantitative estimate of the working range was made by differentiating the plot of slope versus refractive state and selecting the points between which the absolute value of the gain (rate of change of slope with refractive error) was greater than 0.15. This was done with DPlot shareware softwareTM. This choice of the limiting minimum gain of 0.15 was arbitrary, but it provided a metric for comparison between conditions. The actual working range is defined by the particular camera system being used. Another factor in defining the working range is the dead zone in which no changes in profile slope with re-

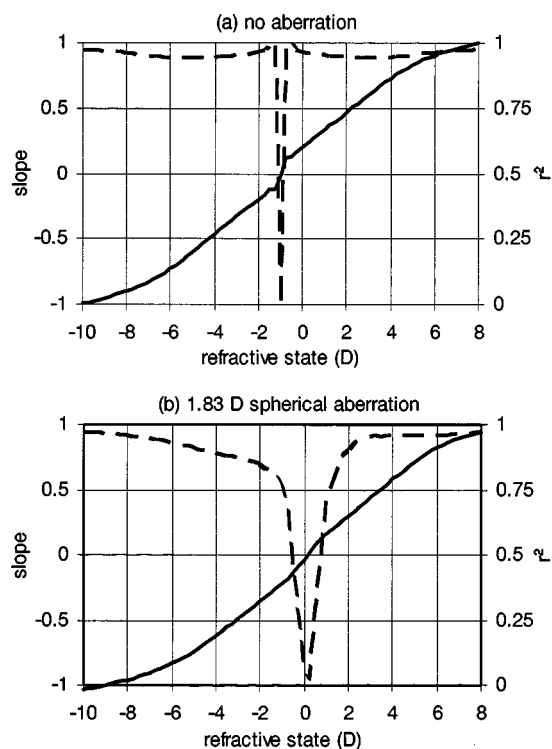


Fig. 7. Plots of slope versus refractive state for an eccentric photorefractor with an extended source made up of point light sources at 0, 3, ..., 30 mm. The solid curves represent the slope of the intensity profile. The dashed curves represent the r^2 value for the slopes best fitted to the calculated intensity profile. The use of a light source at 0 mm eccentricity eliminates the dead zone, even for the no-aberration case. Extension of the source to a 30 mm maximum eccentricity increases the working range. The working range is nearly twice that of the range for the maximum eccentricity of 14 mm used in Fig. 5. The quality of the fit is excellent over most of the working range when the larger extended source is used.

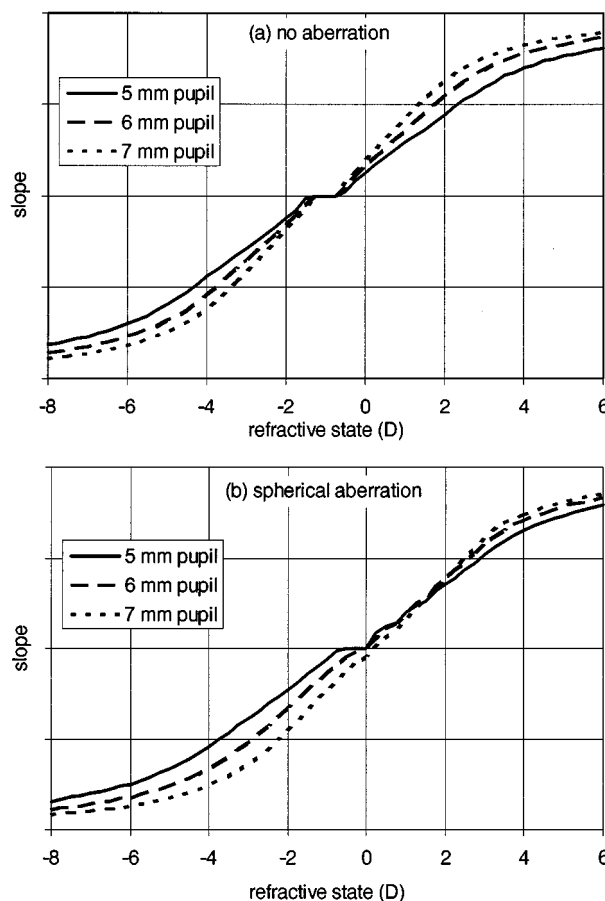


Fig. 8. Effect of pupil size on gain. Both plots show slope as a function of refractive state for three pupil sizes. All slope values have been scaled by the same value. The gain with the 7-mm pupil is the greatest, and it decreases with decreasing pupil diameter. The gain is highest for the 7-mm pupil since more light can enter and exit the eye. When spherical aberration is present in the eye, similar changes in gain occur, and the curve is also shifted horizontally toward the optimal focal state for the amount of aberration present. Differences of more than 1 D in refractive state occur at the ends of the working range.

fractive state are observed. The dead zone generally occurs for refractive states that place the far point of the eye at or near the camera position. Refractive-state changes are undetected within this region.⁴

The plots of slope versus refractive state for different pupil sizes are shown on Fig. 8. The slopes were all normalized with the same factor. Table 1 is a summary of the important results from all the figures and the corresponding working ranges.

4. DISCUSSION

A. Effect of Light Source

The nature of the light source is an extremely important aspect of photorefractor designs, particularly those that measure the slope of the intensity profiles. A comparison of point source versus extended source models can be done by comparing Fig. 4 with the remaining Figs. 5–8 (extended sources). The obvious conclusion is made that the extended source significantly increases the effective range and the linearity of the gain. The empirical work

by Schaeffel *et al.* demonstrating that their instrument is linear over ± 5 D range⁹ is confirmed by this model.

With a point light source the gain is not linear except over a short range of ± 1 D from the camera distance. For refractive states beyond this range the gain quickly goes to 0. This quick reduction in gain is referred to as saturation. The point light source is ineffective in a photorefractor because of its limited working range combined with a large dead zone.

B. Effect of Spherical Aberration

In an eye with spherical aberration, if an extended source is used the change in slope with refractive error still maintains its linearity with nearly the same gain as the no-aberration case (see Figs. 5 and 7). In fact, the presence of aberrations in the eye results in the loss of the region where no light distribution is observed (dead zone). That is, when the eye is focused near the camera, the presence of aberrations leads to small slope values that vary linearly with refractive state. However, although the gain is more constant, the quality of the fit for an eye with aberrations is worse than the no-aberration case over the entire working range. The fit is also dependent on whether the refractive errors are hyperopic or myopic.

The entire curve of slope versus refractive error is shifted toward hyperopia for an eye with positive spherical aberration. Theoretical predictions for an eye with no aberration show that the slope will be zero when the eye is focused on the camera (-1 D). For 1.83 D of spherical aberration the slope is zero at $+0.2$ D, corresponding to a shift of approximately 1.2 D toward hyperopia [Figs. 4(b), 5(b), and 7(b)]. This shift is in a direction consistent with the best defocus state that compensates for the extra myopia at the edges of the pupil.²⁴ This finding was confirmed by calculating how much defocus is required to

minimize the rms aberration across the meridian.²⁴ The optimal defocus to minimize the rms wave-front aberration for an eye with 1.83 D spherical aberration at the edges of the pupil was found to be 1.1 D with a MATHCADTM program. Therefore the shift of the slope caused by the aberrations roughly corresponds to the optimal defocus state caused by the aberration. In other words, the eccentric photorefractor measures the best focus of the eye on the basis of the minimum rms aberration. This amount of shift is not exact, however, and is dependent on the specific refractor configuration. It has been suggested that the eye shifts its subjective focal plane toward this optimal focal plane to correct for aberrations.²⁵

The effects of aberrations apply for both extended and point light sources, but with point light sources the working range is less.

C. Effect of Asymmetric Aberrations

It was shown by Roorda *et al.*¹⁶ that if asymmetric aberrations are present, the shape of the intensity profile observed in the pupil is dependent on the circumferential position of the eccentric light source (i.e., nasal or temporal eccentricity). In an eye with no aberrations or only symmetrical aberrations, the shape of the profile is independent of whether the eccentric source is on either of the diametrically opposite sides of the camera aperture.

The asymmetric aberrations of a single eye measured with the modified Ivanoff apparatus were used to model the effects of asymmetric aberrations. The photorefractor results were predicted for a light source on either side (temporal or nasal) of the camera aperture.

The change in slope with refractive error was linear over a large range with the extended source. The important difference was seen in the change in gain between

Table 1. Summary of Results for All Light Source Configurations

Figure	Light Source	Aberration	Working Range	Dead Zone
4(a)	Point source at 2 mm	No aberration	-2.5 to -1.25 (myopic range) -0.75 to 0.5 D (hyperopic range)	0.5 D
4(b)	Point source at 2 mm	1.83 D positive spherical aberration	-2 to 1.25 D	0 D
4(c)	Point source at 8 mm	No aberration	-4.5 to -2 D (myopic range) 0 to 2.5 D (hyperopic range)	2 D
4(d)	Point source at 8 mm	1.83 D positive spherical aberration	-3.5 to 0.5 D (myopic range) 1.5 to 3.25 D (hyperopic range)	2 D
5(a)	Multiple sources at 2, 5, 8, 11, and 14 mm	No aberration	-4.5 to -1.25 D (myopic range) -0.75 to 2.5 D (hyperopic range)	0.5 D
5(b)	Multiple sources at 2, 5, 8, 11, and 14 mm	1.83 D positive spherical aberration	-3.5 to 3.5 D	0 D
5(c)	Multiple sources at 2, 5, 8, 11, and 14 mm	AR, left eye	-4.5 to 3.25 D	0 D
5(d)	Multiple sources at 2, 5, 8, 11, and 14 mm	AR, left eye	-4 to 2.75 D	0 D
7(a)	Multiple sources at 0, 3..., 30 mm	No aberration	-6.25 to 4.25 D	0 D
7(b)	Multiple sources at 0, 3..., 30 mm	1.83 D positive spherical aberration	-5.25 to 5.25 D	0 D

^a The summary is for a photorefractor working distance of 1 m. The criterion for the working range are the edges of the dead zone and the limits within which the gain is greater than 0.15.

the nasal and the temporal sources. For the particular aberration modeled, the temporal source [Fig. 5(c)] had a slower change in profile slope with refractive error than did the nasal source [Fig. 5(d)] for an extended source. Similar effects were observed for the point light sources, but these are not shown. A dependence of the gain on the circumferential position of the source has obvious implications for calibration since the refractive-state estimation will change with the side of the source or with the eye that is being measured.¹⁵ In general, the quality of the fits for the particular aberration modeled are poor across the working range.

A recently presented technique averages the refractive-state estimate obtained from either side of the meridian of the camera.²⁶ Figure 6 shows the results of averaging the slope obtained from both sides for the particular aberrations in our model. It shows that when both sides are averaged, the gain is comparable to that in the no-aberration and symmetrical-aberration cases.

D. Effect of Changing the Source Eccentricity on the Working Range

The sensitivity of a conventional eccentric photorefractor is controlled by the eccentricity of the light source and the distance of the eye from the camera. For a fixed camera distance, an increase in eccentricity increases the size of the dead zone while allowing refractive-state estimations at higher refractive states.⁴ Slope-based photorefractors operate on the same principles. A smaller eccentricity point source gives a smaller dead zone and working range for refractive-state changes near the camera position. This can be seen by comparing Figs. 4(a) and 4(b) (2 mm eccentricity) with Figs. 4(c) and 4(d) (8 mm eccentricity). In fact, if a point source is at zero eccentricity there is infinite gain and instant saturation, which means that the slope of the profile reverses for a far point on either side of the camera but no change in slope is observed with increases in refractive state. With a point source at 8 mm eccentricity the size of the dead zone increases significantly and the working range is limited to high myopic and hyperopic refractive states. Furthermore, with the high eccentricity the linearity of the intensity profiles is less than for point sources at lower eccentricity.

The extended source takes advantage of the entire range of the light source. The proximal edge of the source (at small eccentricity) allows sensitivity to small amounts of defocus while the distal edge (at high eccentricity) increases the range. The optimal photorefractor design is one with the largest possible extended source. The size of the eccentric light source should be limited only to the extent necessary to minimize light exposure levels and instrument cost and to obtain a desired sensitivity and range. For example, if one is interested only in refractive errors within ± 5 D, there is no need to extend the eccentricity beyond the maximum eccentricity that provides this range.

Figure 7 shows a simulation of a source extending from 0 to 30 mm. The simulation shows that there is no dead zone, even when an eye without aberrations is tested, and the working range covers more refractive states than any other configuration that has been modeled.

E. Dependence of Gain on the Pupil Size

It is important that the calibration of a photorefractor be relatively insensitive to changes in pupil size. If this were not the case, then calibrations would have to account for effects of pupil size. The slope-based photorefractor measures the intensity changes across the pupil. As the pupil decreases in size, the amount of light able to enter the eye and diffusely reflect back to the camera decreases significantly. However, the slope of the intensity profile for smaller pupils is also measured over a shorter length (determined by the pupil diameter). The simulations of Figs. 8(a) and 8(b) show that the pupil size has an effect on the gain. Although the two effects of light loss and reduced pupil diameter tend to cancel each other out, they do not result in the same function. If a calibration for a smaller (5-mm) pupil were applied directly to slopes measured for a 7-mm pupil, errors in refractive-state estimation of over 1 D could occur (Fig. 8). When aberration is present [as seen in Fig. 8(b)], the gain curves are shifted with increasing pupil diameter. This is because the aberrations are increasing with pupil diameter, which in turn shifts the optimal defocus state for the eye. These results indicate that an accurate slope-based eccentric photorefractor would still require a calibration that would account for the expected range of pupil sizes.

F. Comparison with Previous Empirical Investigations

Schaeffel *et al.* have published calibration curves for four amphibian and mammalian species.¹⁵ The changes in slope with refractive error give results that are remarkably similar to those of our simulations. In general, the linearity of the slope change was over a range of ± 8 D. The particular refractor configuration used had five rows of LED's from 2 to 22 mm. The range of the instrument was improved over the previous design used in the 1993 paper by an increase in the maximum eccentricity from 17 to 22 mm.⁹ The differences in gain between the species were likely due to differences in retinal reflectivity, and we expect that deviations from linearity in two of the species (*Rana pipiens* and *Rana temporarium*) were due to aberrations in the eye.

Andison *et al.* used the same device as Schaeffel but at a 30-cm working distance to measure accommodation in fish.²⁷ The working range in that case was increased to ± 15 D. To increase the working range further and correct for nonlinearity of the gain curve, the instrument was calibrated by fitting a third-order curve to the measured change in slope with refractive state.

5. CONCLUSIONS

This paper provides a theoretical basis for describing the effects of different light sources and the effects of monochromatic aberrations on slope-based photorefractors. The study provides a means of comparing and simulating new photorefractor designs with analysis metrics that include gain, working range, dead zone, and linearity of the best-fit slopes.

The clear conclusion from this investigation is that the extended light source is a better choice than a point light source for eccentric photorefractors that base estimations of refractive error on the slope of the intensity profile.

The use of an extended source increases the working range and improves the quality of the fit over this working range, with increasing uncertainty for low refractive errors.

The presence of aberrations in the eye reduces the quality of the slope estimation and thus reduces the accuracy of the refractive-state estimation. With spherical aberration present, the curve maintains the same gain characteristics as for eyes with no aberration but shifts to the defocus that approximately compensates for the aberration.

Asymmetric aberrations cause the most difficulties for photorefractive. The gain is dependent on whether the source is on one or the other side of the aperture. Asymmetric aberrations in the eye are as likely as symmetrical ones,^{17,18} so this poses a real concern. The gain was made comparable to those of the symmetrical and the no-aberration cases by averaging the slope obtained with a source on either side of the camera. The photorefractor model of Gekeler *et al.*,²⁶ which averages the slope from sources on either side of the meridian, is therefore the best possible technique for dealing with asymmetric aberrations.

Another concern is the change in gain with pupil size. This study has shown that the calibration is dependent on the pupil size and that if this dependence is not considered, errors in refractive state of more than 1 D may occur.

The Fortune Optical (Tomey ViVA) uses small infrared light sources offset from three sides of the camera aperture.¹⁰ We have measured the eccentricity to be approximately 7 mm. Because of the light source configuration, it is not surprising that the Tomey ViVA videorefractor was shown to have a limited working range of only ± 3 D (Ref. 10) and poor correlations between expected and measured refractive states. The quality of the fits to the intensity profile slopes and consequently the estimations of the refractive state are expected to be poor because a small light source is used. The estimations for low refractive errors were often compromised by "irregular intensity profiles."¹⁰ An extended source over a large range can correct some of these problems.

The convenience of eccentric-photorefractive devices is recognized in the testing of infants and children in both research and clinical fields. This is particularly true for the slope-based photorefractors since they are relatively inexpensive and are easily automated. However, the accuracy of these techniques has been questioned and has been shown in our research and in some of the literature to be unreliable. These optical simulations are important to determine optimal configurations for such instruments in attempts to improve their performance. It is also important that the monochromatic aberrations of the eye be incorporated into the model, since relatively large amounts are usually present in the human eye at moderate pupil sizes.

ACKNOWLEDGMENT

The authors are grateful for support from Natural Sciences and Engineering Research Council, Canada.

Address correspondence to Austin Roorda, Center for Visual Science, University of Rochester, Rochester, New York 14627; email: aroorda@cvs.rochester.edu.

REFERENCES

1. K. Kaakinen, "A simple method for screening of children with strabismus, anisometropia or ametropia by simultaneous photography of the corneal and fundus reflexes," *Acta Ophthalmol.* **57**, 161–171 (1979).
2. B. Rosengren, "A method of skiascopy with the electric ophthalmoscope," *Acta Ophthalmol.* **15**, 501–511 (1937).
3. K. Kaakinen, H. O. Kaseva, and K. Eeva-Raija, "Mass screening of children for strabismus or ametropia with two flash photoskiagraphy," *Acta Ophthalmol.* **64**, 105–110 (1986).
4. W. R. Bobier and O. J. Braddick, "Eccentric photorefractive: optical analysis and empirical measures," *Am. J. Optom. Physiol. Opt.* **62**, 614–620 (1985).
5. H. C. Howland, "Optics of photoretinoscopy: results from ray tracing," *Am. J. Optom. Physiol. Opt.* **62**, 621–625 (1985).
6. W. R. Bobier, "Eccentric photorefractive: a method to measure accommodation of highly hypermetropic infants," *Clin. Vision Sci.* **5**, 45–66 (1990).
7. H. Uozato, M. Saishin, and D. L. Guyton "Refractive assessment of infants with infra-red video-refractor PR-1000," *Invest. Ophthalmol. Visual Sci.* **4**, 1238 (1991) (abstract).
8. M. C. W. Campbell, W. R. Bobier, and A. Roorda, "Effect of monochromatic aberrations on photorefractive patterns," *J. Opt. Soc. Am. A* **12**, 1637–1646 (1995).
9. F. Schaeffel, H. Wilhelm, and E. Zrenner, "Inter-individual variability in the dynamics of natural accommodation in humans: relation to age and refractive errors," *J. Physiol. (London)* **461**, 301–320 (1993).
10. A. M. Thompson, T. Li, L. B. Peck, H. C. Howland, R. Counts, and W. R. Bobier, "Accuracy and precision of the Tomey ViVA Infrared Photorefractor," *Optom. Vis. Sci.* **73**, 644–652 (1996).
11. H. Uozato, M. Saishin, and H. Hirai, "Photorefractor PR-2000 for refractive screening of infants," *Invest. Ophthalmol. Visual Sci.* **4**, 861 (1993) (abstract).
12. H. Uozato, M. Saishin, and Y. Fukuma, "The photorefractor PR-1000 for refractive screening of infants," in *Current Aspects in Ophthalmology, Vol. 1*, K. Shimizu, ed. (Excerpta Medica, London, 1992), pp. 704–708.
13. F. Schaeffel, L. Farkas, and H. C. Howland, "Infrared photoretinoscope," *Appl. Opt.* **26**, 1505–1509 (1987).
14. F. Schaeffel and H. C. Howland, "Measurement of pupil size, direction of gaze, and refractive state by on-line analysis of digitized video images," in *Noninvasive Assessment of the Visual System*, Vol. 1 of 1991 OSA Technical Digest Series (Optical Society of America, Washington D.C.), pp. 76–79.
15. F. Schaeffel, G. Hagel, J. Eikermann, and T. Collett, "Lower-field myopia and astigmatism in amphibians and chickens," *J. Opt. Soc. Am. A* **11**, 487–495 (1994).
16. A. Roorda, M. C. W. Campbell, and W. R. Bobier, "Geometrical theory to predict eccentric photorefractive intensity profiles in the human eye," *J. Opt. Soc. Am. A* **12**, 1647–1656 (1995).
17. M. C. W. Campbell, E. M. Harrison, and P. Simonet, "Psychophysical measurement of the blur on the retina due to optical aberrations of the eye," *Vision Res.* **30**, 1587–1602 (1990).
18. G. Walsh, W. N. Charman, and H. C. Howland, "Objective technique for the determination of monochromatic aberrations of the human eye," *J. Opt. Soc. Am. A* **1**, 987–992 (1984).
19. A. Roorda, *Double Pass Reflections in the Human Eye* (Ph.D. dissertation, University of Waterloo, Waterloo, Canada, 1996).
20. G. A. Fry and M. Alpern, "The effect of a peripheral glare

- source on the apparent brightness of an object,” *J. Opt. Soc. Am.* **43**, 189–195 (1953).
21. I. J. Hodgkinson, P. B. Greer, and A. C. B. Molteno, “Point-spread function for light scattered in the human ocular fundus,” *J. Opt. Soc. Am. A* **11**, 479–486 (1994).
 22. F. C. Delori and K. P. Pflibsen, “Spectral reflectance of the human ocular fundus,” *Appl. Opt.* **28**, 1061–1077 (1989).
 23. I. J. Hodgkinson, K. M. Chong, and A. C. B. Molteno, “Photorefraction of the living eye: a model for linear knife edge photoscreening,” *Appl. Opt.* **30**, 2263–2269 (1991).
 24. W. J. Smith, *Modern Optical Engineering* (McGraw-Hill, New York, 1990).
 25. C. Cui, M. C. W. Campbell, W. N. Charman, and L. Voisin, “Reducing aberration at the fovea by defocus,” in *Ophthalmic and Visual Optics*, vol. 3 of 1993 OSA Technical Digest Series (Optical Society of America, Washington, D.C.), pp. 164–167.
 26. F. Gekeler, J. Wattam-Bell, and F. Schaeffel, “Measurement of human astigmatism with infrared photoretinography,” *Invest. Ophthalmol. Visual Sci.* **37**, 725 (1996) (abstract).
 27. M. E. Andison, J. G. Sivak, and M. G. Callender, “Convergence and accommodation in a teleost fish, the Oscar,” *Invest. Ophthalmol. Visual Sci.* **37**, 162 (1996) (abstract).
 28. M. Born and E. Wolf, *Principles of Optics*, 6th ed. (Pergamon, Oxford, 1980).